APPLICATION OF CFD TO THE FUSELAGE AERODYNAMICS OF THE EC145 HELICOPTER. PREDICTION OF UNSTEADY PHENOMENA AND OF THE TIME AVERAGED INFLUENCE OF THE MAIN ROTOR.

by

A. D'Alascio and A. Berthe
EUROCOPTER DEUTSCHLAND GmbH, 81663 München, Germany

F. Le Chuiton
DLR, Deutsches Zentrum für Luft und Raumfahrt e.V. Braunschweig, Germany

APPLICATION OF CFD TO THE FUSELAGE AERODYNAMICS OF THE EC145 HELICOPTER. PREDICTION OF UNSTEADY PHENOMENA AND OF THE TIME AVERAGED INFLUENCE OF THE MAIN ROTOR.

A. D'Alascio and A. Berthe
EUROCOPTER DEUTSCHLAND GmbH, 81663 München, Germany

F. Le Chuiton
DLR, Deutsches Zentrum für Luft und Raumfahrt e.V. Braunschweig, Germany

Helicopter fuselages are often characterised by complex surface shapes which deviate the flow and strongly modify its structure, thus generating early transition and many local separations with their inherent vortex shedding. The early flow separation on blunt fuselage shapes may generate unsteady vortex structures which can be captured by the numerical simulation only by solving the URANS (Unsteady Reynolds-Averaged Navier-Stokes) equations. Moreover, the mutual interactions between rotor and fuselage have strong influence on helicopter performance and handling qualities. In order to predict these complex flow phenomena accurately, numerical methods based on the solution of the Navier-Stokes equations with a sufficiently detailed grid, time interval and turbulence model have to be applied. Furthermore both multiblock and Chimera overlapping mesh techniques need to be mastered in parallel, to allow robustness and quality of the numerical solution, while minimising preparation and CPU time for an industrial application [1].

The paper will focus on the industrial use of CFD (Computational Fluid Dynamics) at EUROCOPTER with the purpose of studying the aerodynamic properties of the EC145 helicopter fuselage. A comparison between numerical prediction and wind tunnel measurements will be made for the isolated fuselage configuration and the effects of the Actuator Disk (AD) on local and global flow quantities will be shown.

Nomenclature

$C_n M^2$	- sectional force coefficient in normal direction to the blade chord
$C_t M^2$	- sectional force coefficient in blade chord direction
C_P / σ	- rotor power coefficient $= P/(\rho_\infty (\omega R)^3 \pi R^2 \sigma)$
C_T / σ	- rotor thrust coefficient $= T/(\rho_\infty (\omega R)^2 \pi R^2 \sigma)$
C_X	- drag coefficient $= D/(1/2 \rho_\infty v_\infty^2 S)$
C_Z	- lift coefficient $= L/(1/2 \rho_\infty v_\infty^2 S)$
D	- drag and cylinder diameter
L	- lift
$M_{\omega R}$	- rotational tip Mach number
M_∞	- free stream Mach number
P	- rotor power
R	- rotor radius
Re	- Reynolds number $= \rho v l / \mu$
Re_D	- Cylinder Reynolds number $= \rho_\infty v_\infty D / \mu_\infty$
T	- rotor thrust
TPL	Total Pressure Losses $= 1 - P_{TOT} / P_{TOT\infty}$
$y^+ = \rho_{wall} u_t y / \mu_{wall}$	being u_t the local tangential velocity and y the vertical direction

Greek letters

α	- angle of attack
β	- side slip angle
υ	- cinematic viscosity $= \mu / \rho$
μ	- dynamic viscosity
μ	- advance ratio $= M_\infty / M_{\omega R}$
ω	- rotor angular velocity
ρ	- air density
σ	- rotor solidity $= nc / \pi R$ being n the number of blades and c the blade chord

Acronyms

AD	Actuator Disk
CAD	Computer Aided Design
CFD	Computational Fluid Dynamics
LEA	Linear Explicit Algebraic stress model
PIV	Particle Image Velocimetry
URANS	Unsteady Reynolds-Averaged Navier-Stokes

Subscripts

0	- mean or nominal value
∞	- free stream value

1 Introduction

As time-to-market for the design and development of a new helicopter or an upgrade of an existing one has to be decreased to be competitive in the world market, there is a pressing need for improved aerodynamic methodologies capable of analysing the flow field around helicopter components such as main rotor or fuselage and empenage in various flight conditions.

Flight tests are extremely expensive and time consuming while the solutions found are often palliatives rather than optimised configurations. The wind tunnel methodology can be more efficient for conventional problems such as fuselage drag reduction but many low speed interactional conditions have been found difficult to test with sufficient confidence [2]. Over the last few years CFD methods developed by the research community have rapidly matured and are now available as powerful commercial products. Solutions with engineering accuracy for surface pressure can be obtained for realistic three-dimensional configurations such as those applicable to complete commercial aircraft. The helicopter industry is therefore increasingly using CFD methods by incorporating them in its design environment in order to reduce the number of wind tunnel tests and to increase the number of configurations being explored numerically [3][4].

Helicopter fuselage shapes present particularly complex surfaces which deviate the flow and strongly modify its structure, thus generating early transition and many local separations with their inherent vortex shedding. Moreover, the mutual interactions between rotors and fuselage have strong influence on helicopter performance and handling qualities. In order to predict these complex flow phenomena accurately, numerical methods based on the solution of the Navier-Stokes equations with a sufficiently detailed grid, time interval and turbulence model have to be applied. Furthermore both multiblock and Chimera overlapping mesh techniques need to be mastered in parallel, to allow robustness and quality of the numerical solution, while minimising preparation and CPU time for an industrial application.

The paper presents the comparison between CFD prediction results and wind tunnel measurements in terms of global integrated quantities, *i.e.* drag and lift, about the EC145 isolated fuselage in low speed level flight. Both steady and unsteady computations have been performed. Furthermore the effect of the actuator disk boundary condition, simulating the time-averaged influence of the main rotor induced velocity field on the fuselage will be evaluated in high speed level flight.

2 The FLOWer flow solvers

The FLOWer flow solver [5],[6] is the Euler/Navier-Stokes code developed by DLR, which is being enhanced within the frame of the Franco-German "CHANCE" research project supported on the German side by the Ministry of Economics. It solves the compressible, three-dimensional unsteady Reynolds-averaged Navier-Stokes equations on block structured meshes around bodies in arbitrary motion. FLOWer implements two different spatial discretisation schemes, based on finite volume formulation, where the flow variables are located either at the vertices or at the cell centres.

The baseline method employs a central space discretisation with artificial viscosity and an explicit five stage Runge-Kutta time integration scheme. Local time-stepping, implicit residual smoothing and multigrid can be used to accelerate convergence. Turbulence is modelled by algebraic or by more general transport equation models, *e.g.* the two equation $k-\omega$ model. Low velocity preconditioning, deforming meshes and the Chimera technique are also available.

2.1 The Actuator Disk model

The main rotor is replaced by an infinitely thin disc, under which source terms are specified in order to mimic the influence of the rotor on the fluid. This disc is practically accounted for as an inter-block cut boundary during the mesh generation process. Then a force distribution, provided for instance by a previous isolated rotor computation, can be interpolated as source terms on the surface mesh of the disc: the force itself in the momentum equation and its corresponding energy in the energy equation. As such, this formulation is readily amenable to low-velocity preconditioning and has been integrated in a parallel framework. For details the reader is referred to [7].

3 The EC145 fuselage in forward flight

Nowadays the aerodynamic department of helicopter manufacturers uses CFD for the flow field analysis of fuselage as well as of isolated rotors. In the domain of fuselage aerodynamics, CFD is currently in use at EUROCOPTER for several applications such as:

- supplement the wind tunnel tests and provide surface pressure distribution as input for stress analysis of fuselage structure components *i.e.* doors, horizontal stabilisers, endplates etc.[2];
- optimise the aerodynamic design of fuselages and fuselage parts *i.e.* air inlet geometry, engine outlet etc.

3.1 Aerodynamic Design of the EC145

The EC145 twin engine helicopter, depicted in Figure 1, is equipped with a 4-bladed main rotor, a conventional 2-bladed tail rotor and two landing skids. The shape of the rear side of the fuselage is formed blunt by a backdoor which allows the loading from the back. Such configuration makes the EC145 particularly suited to security and rescue missions, but it definitely complicates the flow field structure, and in consequence the aerodynamic predictions and analysis. In fact the steep junction between the fuselage body and the tail boom is responsible for a separated flow region which might give birth to unsteady vortex structures which are shed downstream (von Karman vortices). In this case the use of the most sophisticated turbulence models is mandatory to accurately predict the fuselage drag. In addition, when unsteady phenomena occur, the solution of the URANS equations is necessary.

Figure 1: EC145 helicopter (CATIA v.4 model)

3.2 Flight conditions and experimental data

Table 1 reports the two flight conditions selected for the CFD analysis. The first is a low speed at 40m/s whereas the second is a high speed at about 70m/s.

Case	V_∞	M_∞	$\mathrm{Re}\,[10^6]$
	[m/s]	[-]	[-]
Low speed	40	0.117	2.73
High speed	69.75	0.208	4.50

Table 1: Free stream conditions for the two considered test cases.

The low speed flight condition has been extracted from the wind tunnel campaign carried out at EC Marignane (France) in 1997, whereas the high speed condition stems from a large flight test measurement campaign carried out at ECD Donauwörth (Germany) in 1999 in order to certify the EC145 (under the former name BK117-C2). During the wind tunnel campaign, all global values, *i.e.* lift, drag, side force and the three pitch, roll and yaw moments were recorded at different angles of attack α and side slip angles β. The flight test data recorded during the flight campaigns consist of the helicopter weight, the total power measured at the engine drive shaft, the tail rotor power measured at the tail rotor drive shaft and all flight conditions.

4 The CFD simulations

In order to make a first assessment of the CFD predictions a comparison between the low speed wind tunnel data and some FLOWer results has been carried out. A number of steady and unsteady computations about the isolated EC145 fuselage was performed by changing just the fuselage angle of attack and keeping the other flow field and numerical parameters unchanged. Although more expensive than the standard Wilcox k-ω turbulence model, the LEA (Linear Explicit Algebraic stress model) modification to the standard k-ω model has been used in all computations, because of its better behaviour in presence of separated regions, e.g. stalled blades or blunt bodies. The laminar-turbulent transition line has not been assigned in any computation, therefore all FLOWer results are fully turbulent.

After assessing the CFD results on the isolated fuselage in low speed flight a second run has been performed in high speed level flight by applying the actuator disk boundary condition. The load distribution applied on the actuator disk surface has been derived from a previous Navier-Stokes FLOWer computation about the ATR-A 4-bladed isolated rotor [8]. The trim conditions for this high speed forward flight test case have been computed by means of the aeromechanics code CAMRAD II [9].

4.1 Numerical description

A CFD analysis procedure is usually composed of three phases: a pre-processing, the flow field computation and a data post-processing and analysis. This section describes briefly the pre-processing activity. It consists basically in the generation of a volume mesh modelling the computational domain and in the definition of the flow solver operational parameters.

The volume grid generation started from the EC145 surface mesh of Figure 1 already available, in the design department, as a CAD CATIA model. This structural model has been cleaned and simplified by completely removing main and tail rotor, landing gear, antennas and handles. The air intakes and jet exhausts have been closed and all gaps between adjacent surface patches have been repaired. Figure 2 shows the aerodynamic "water tight" CATIA model obtained after the above

mentioned activity. The aerodynamic CATIA model has been then imported into the volume grid generator ICEM-Hexa. The resulting structured multi-block Navier-Stokes mesh about the isolated fuselage is composed of 64 blocks, 4.9 million nodes and allows 3 levels of multigrid. The topology structure is a C-O, with the C-structure in the longitudinal direction and the O-structure in the transversal one. A boundary layer grid has also been generated around the whole surfaces. Figure 3 shows the middle co-ordinate grid plane. The C-topology structure in the grid longitudinal direction is visible here.

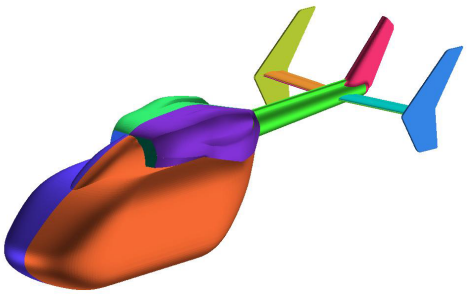

Figure 2: EC145 isolated fuselage (CATIA v.4 aerodynamic model)

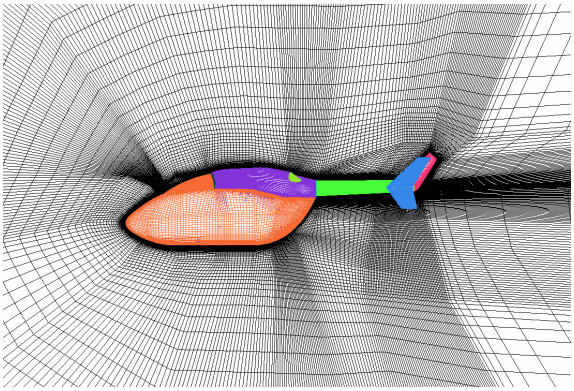

Figure 3: ICEM-Hexa mesh about the EC145 isolated fuselage: middle plane.

In both flight conditions of Table 1 the calculated y^+ on the body surfaces have a maximum value of 1.0, therefore the grid is fine enough to capture the strong gradients occurring in the boundary layer.

For the CFD simulation of the fuselage with the main rotor modelled as an actuator disc, an auxiliary mesh around the AD has been generated and is made of 4 blocks and 430,000 points. The rotor portion has been gridded by two cylindrical blocks (top and bottom) to allow for mesh regularity and two additional blocks (top and bottom) have been fitted in the core portion to avoid grid singularities.

The Chimera interpolation algorithm on overlapping grids has been used to assure the information exchange between the Chimera boundaries. The resulting grid system depicted in Figure 4 is composed of the isolated fuselage as background grid and the AD mesh as embedded child grid.

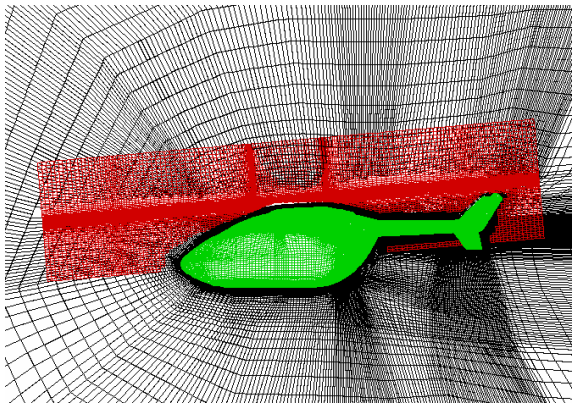

Figure 4: Chimera grid system: Background grid around the EC145 isolated fuselage, child grid around the Actuator Disc.

4.2 Flow analysis: The isolated fuselage in low speed forward flight.

The section presents the comparison between the numerical results and the low speed wind tunnel data in terms of drag $\mathbf{C_X}$ and lift $\mathbf{C_Z}$ coefficients. Several computations have been performed by changing the angle of attack α of the fuselage while keeping all other free stream parameters unchanged. Polar curves have been thus generated. Table 2 reports the parameters of the performed three sets of FLOWer runs: the first steady test case has been run on the wind tunnel model geometry, whereas the other two, one steady and the other unsteady, on the real scale configuration. The Navier-Stokes structured code FLOWer has been run for all test cases using 3 levels of multigrid on a 6-processor SGI R12000 work station and applying the LEA k-ω turbulence model.

Run	V_∞	α (Positive nose –up)	Scale
	[m/s]	[degree]	[-]
Steady	40	-12°, -6°, 0°, 6°	Model
Steady	40	-12°, -6°, 0°, 6°	Full
Unsteady	40	-12°, 0°	Full

Table 2: Flower runs performed in low speed forward flight.

Figure 5 and Figure 6 show the comparison between the wind tunnel measurements (black dots) and two FLOWer computations (in green the wind tunnel model and in blue the full scale helicopter) in

terms respectively of drag C_X and lift coefficient C_Z versus angle of attack α. An error bar has been drawn on both measurement and predictions. The measurement errors have been computed by using empirical formulas which take into account uncertainties introduced during the wind tunnel data post processing. The uncertainties on the numerical results are due to some convergence oscillations. In fact the convergence behaviour of all steady computations is characterised by a first decrease of all equation residuals down to two orders of magnitude and a subsequent oscillation around a constant value. The same behaviour has been encountered for the lift and drag convergence history. Therefore the prediction values of Figure 5 and Figure 6 represent the mean value of this oscillation, whereas the error bar shows the amplitude of the oscillation. It must be mentioned that the contribution to the drag and lift values of the horizontal stabilisers and endplates has been subtracted from the isolated fuselage global values in both predictions and measurements. Therefore Figure 5 and Figure 6 show the contribution of the fuselage cell, tail boom and vertical fin only. This was made necessary because the EC145 final geometry mounted slightly different horizontal stabilisers from the wind tunnel model one.

The FLOWer model scale computation reproduces exactly the wind tunnel measurement campaign, the full scale computation has been added here to show the Reynolds number effect. It is worth to be noticed that the oscillations in the convergence have a bigger effect on the lift values than on the drag, nevertheless the uncertainties remain for both figure very much limited. The agreement between the numerical results and the wind tunnel measurements is definitely satisfactory especially for negative angles of attack (which is the operational region for the angle of attack). A bigger discrepancy occurs at α=6°. This might be partly due to the wind tunnel pylon induced flow on the fuselage bottom surface.

The pylon, placed vertically, connects the wind tunnel floor with the fuselage bottom surface. The balance has been placed at the pylon/fuselage junction. This solution allows to measure only the forces acting on the fuselage, nevertheless the pylon influence on the fuselage, *e.g.* earlier separation and local pressure distribution modifications, cannot be avoided. Actually a bigger induced flow effect should be expected at positive angles of attack. In fact, as shown in Figure 7, at α=0° and 6° the highest negative peak values for the pressure coefficient occur behind the pylon. Therefore the pylon induced flow on the fuselage is expected to have a bigger effect in terms of pressure and friction coefficient distribution and consequently on the drag value at positive angles of attack. An earlier flow separation induced by the pylon might justify then the drag underestimation at α=6°. A simulation in which the wind tunnel pylon is modelled together with the fuselage should be done to prove this assumption.

The comparison between the two FLOWer runs: one on the wind tunnel model scale and the other on the full scale helicopter shows the Reynolds effect on drag and lift: changing the scale from wind tunnel model to full scale, *i.e.* increasing the body dimensions by keeping all other flow parameters unchanged, increases proportionally the Reynolds number. This causes a decrease of the drag (see Figure 5) without modifying considerably the lift (see Figure 6). The discrepancy shown in Figure 6 between the predicted and the measured lift coefficient at α=−12° might be caused by a problem in the measured data for this test point. In fact in this range, *i.e.* for α comprised between −12° and 12° a linear behaviour of the measurements should occur, which is not the case at α=−12°.

Figure 7 shows the comparison, for different angles of attack α, of the FLOWer predictions in terms of pressure coefficient distribution versus X-co-ordinate on the fuselage mid-bottom line. The fuselage bottom contour has also been depicted. A stagnation region towards the fuselage nose and a flow separation (Cp≈0) towards the back door can be noticed. Note as well how the variation of the angle of attack from negative values, *nose down*, to positive values, *nose up*, decreases the negative pressure peak at the nose and increases it at the back of the fuselage.

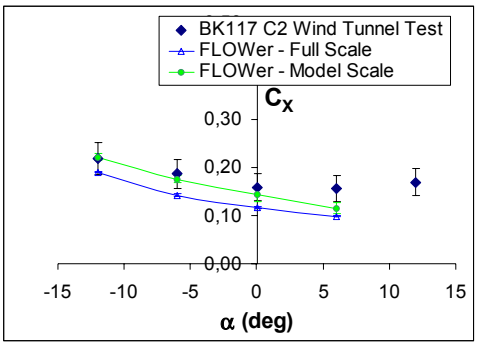

Figure 5: Drag coefficient versus fuselage angle of attack. Fuselage cell, tail boom and vertical fin contributions.

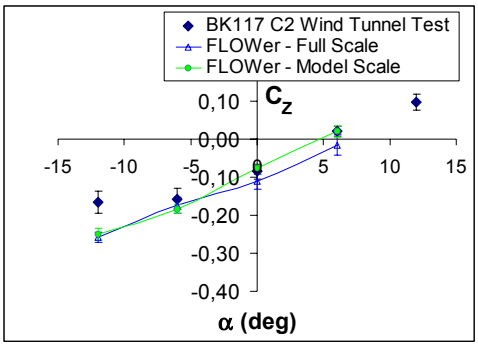

Figure 6: Lift coefficient versus fuselage angle of attack. Fuselage cell, tail boom and vertical fin contributions.

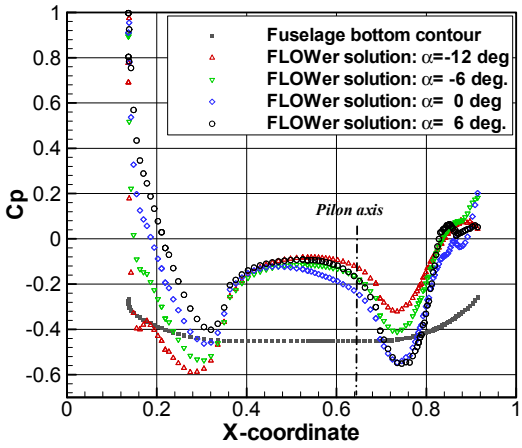

Figure 7: Effect of the angle of attack on the pressure coefficient distribution prediction. (Wind tunnel model scale. Fuselage bottom symmetry plane.)

Preliminary steady and unsteady computations performed about an infinite cylinder showed that when a steady computation is performed while the physical phenomenon is actually unsteady, such as the case of a cylinder at Re_D>40, the convergence residuals, as well as the lift and drag values, present oscillations. Moreover the drag mean value relative to the steady run is different to the one computed during the unsteady run. Indeed the comparison, in terms of drag versus Reynolds number, of Figure 8 between steady and unsteady FLOWer predictions and some wind tunnel data extracted from literature have shown a better prediction for the unsteady runs. The error bar of the measurements show the drag range variation function of the cylinder surface roughness, whereas the predictions error bars are representative of the numerical oscillations for the steady run and of the unsteady variation for the unsteady one.

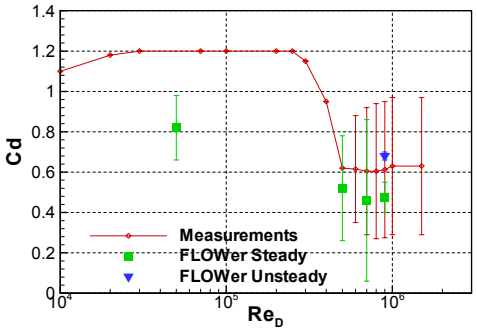

Figure 8: Comparison between FLOWer steady and unsteady runs and wind tunnel measurements around an infinite cylinder. Drag coefficient versus Reynolds number.

The infinite cylinder experiment showed that when an unsteady phenomena occurs, *e.g.* the birth of the von Karman vortex unsteady structures behind blunt bodies, an accurate prediction of the drag and lift requires the introduction of the physical time step in the Navier-Stokes equations, by keeping boundary conditions and numerical parameters unchanged. Therefore two additional unsteady runs about the EC145 isolated fuselage in low speed forward flight have been made, one at an angle of attack of α=0° and the other of α=–12° (see also Table 2).

Figure 9 and Figure 10 show the comparison between steady and unsteady computations in terms respectively of drag and lift coefficients versus angle of attack. The full scale geometry has been used for these computations. The predicted lift and drag refer to the complete configuration, comprising fuselage, tail boom, horizontal stabilisers, vertical fin and endplates. The comparison does not show significant differences between steady and unsteady results. This is certainly due to the fact that the separation region is confined to a relatively small region (if compared to the infinite cylinder test case) of the helicopter back door. In fact the pressure and the skin friction distributions on most of the helicopter surface stabilise quite soon during convergence, while they oscillate on the separated flow region. In this case the solution of the steady N.-S. equations is sufficient to predict the loads acting on the helicopter fuselage, the unsteady equations being necessary when bigger separated areas occur.

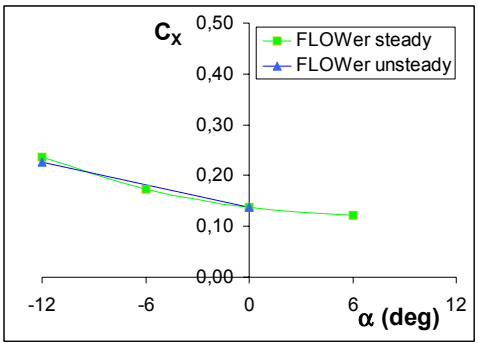

Figure 9: Comparison between FLOWer steady and unsteady runs. Drag coefficient versus fuselage angle of attack. (Full scale model)

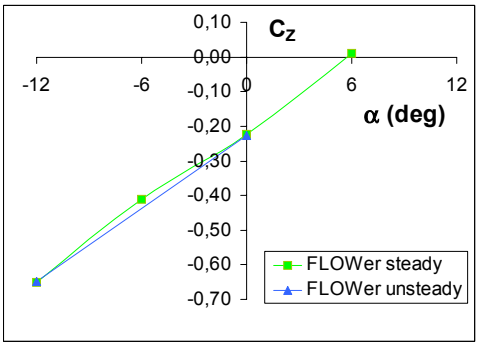

Figure 10: Comparison between FLOWer steady and unsteady runs. Lift coefficient versus fuselage angle of attack. (Full scale model)

4.3 Flow analysis: Fuselage with AD model in high speed level flight.

The section presents the comparison between two numerical predictions. The first has been obtained by solving the N.-S. steady equations about the isolated fuselage in high speed forward flight (see Table 1) at zero angle of attack, whereas the second refers to fuselage plus AD. This last test case has been run in unsteady mode. In fact a first steady run showed considerable oscillations on the lift and drag values during convergence, highlighting the presence of unsteady phenomena possibly related to the AD wake interacting with the fuselage. Therefore it was decided to run FLOWer in unsteady mode too. Considering that the free stream conditions, the FLOWer control parameters and the mesh around the isolated fuselage are the same on both CFD simulations, the comparison between the two solutions will highlight the effect of the actuator disk on the fuselage.

The loads applied on the AD surface have been derived from an already performed Navier-Stokes chimera computation about the isolated 4-bladed rotor, mounted on the EC145 helicopter, in forward flight conditions [8]. In order to validate the accuracy of the CFD solution, a comparison between prediction and the flight test data has been carried out. Figure 11 shows the comparison between flight test data and N.-S. prediction in terms of main rotor power coefficient versus thrust coefficient. The comparison between the numerical results and the flight test data show fairly good agreement for the Navier-Stokes computation. In fact the numerical results show a slight underestimation, with respect to the flight test measurement.

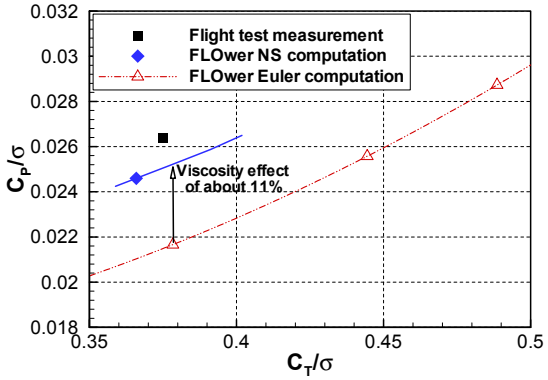

Figure 11: Comparison of CFD results and flight test data: main rotor power versus thrust coefficient.

Figure 12 and Figure 13 show the normal and the tangential force coefficient distributions on the rotor disk plane as computed by FLOWer. These values, once interpolated on the AD surface mesh, constitute the boundary condition assigned on the AD surface, for the test case fuselage plus rotor in high speed forward flight condition.

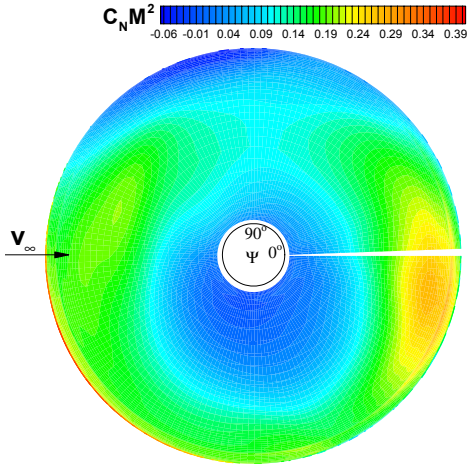

Figure 12: Normal force coefficient distribution on the rotor disk plane

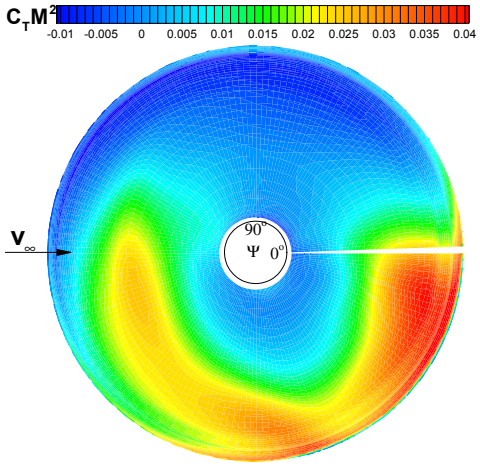

Figure 13: Tangential force coefficient distribution on the rotor disk plane

The isolated fuselage test case was run on 6-processors of an SGI R12000 work station. 48 hours of CPU time were needed to perform 1300 iterations in steady mode. The unsteady test case run at DLR required 15000 iterations on the NEC SX5 super computer. The global lift and drag coefficients have been reported in Table 3. By comparing the fuselage plus AD values obtained by running the steady and unsteady N.-S. equations only a 2% difference is encountered on the drag values, whereas a 10% difference is found on the lift. This shows that the unsteady phenomenon has a bigger impact on the helicopter horizontal stabilisers. In fact, at zero angle of attack, they are responsible for at least 50% of the fuselage total lift. This fact can be verified in the low speed forward flight section by comparing the lift values of Figure 6, relative to the helicopter fuselage without empennage, and of Figure 10,

relative to the complete fuselage. Indeed, the comparison between isolated fuselage and fuselage plus AD shows that the AD induced flow has a negligible effect on the total drag value, but an important one on the lift value, highlighting once more that the AD model might be important in analysing where the rotor wake interacts with the fuselage components, for instance for pith up or tail shake phenomena.

Test case	Mode run	C_X (Drag)	C_Z (Lift)
Isolated fuselage	Steady	0.135	-0.230
Fuselage plus AD	Steady	0.132	-0.294
	Unsteady	0.130	-0.324

Table 3: Lift and drag coefficients for the isolated fuselage and fuselage plus AD runs.

Figure 14 shows the pressure coefficient distribution on the EC145 fuselage for the computation using the AD model (*upper picture*) and without (*lower one)* respectively. Both pictures present the typical stagnation region on the fuselage nose followed by a flow acceleration on the fuselage central part. A deceleration, mainly due to a flow separation and re-attachment, is encountered at the fuselage tail-boom junction. The picture highlights again that the AD relevant influence in such a high speed forward flight condition is limited to the horizontal and vertical stabilisers, and to the endplates.

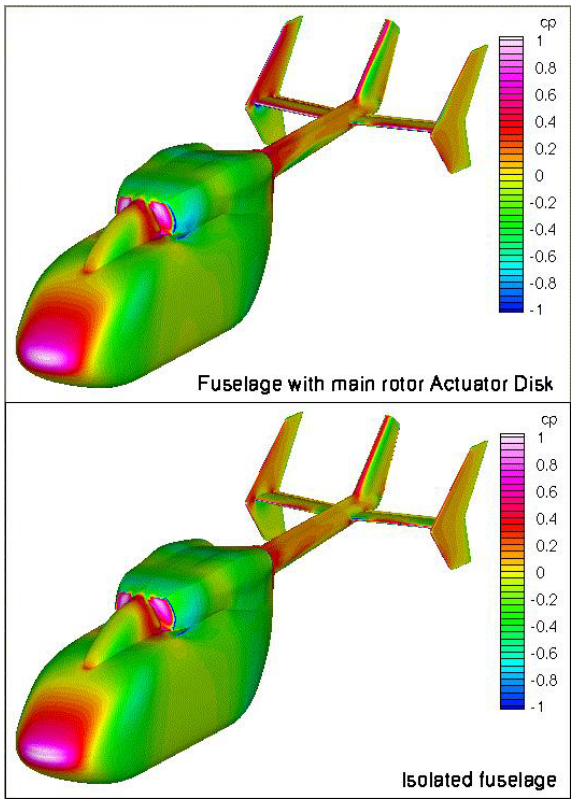

Figure 14: Pressure coefficient distribution on the fuselage, with AD (upper) and without (lower).

Figure 16 and Figure 17 show the comparison between the two FLOWer solutions in terms of pressure coefficient distribution on the fuselage sections depicted in Figure 15. The pressure coefficient plot on the fuselage middle section of Figure 16 shows even more clearly that the AD influence on the fuselage appears more relevant on the tail boom than on the fuselage itself. In hover conditions it would be exactly the opposite. Even more important is the effect on the horizontal stabilisers, as it appears in Figure 17-*top* for the left wing (see Figure 15 Section B) and Figure 17-*bottom* for the right one (see Figure 15 Section C). The AD induced velocity on both left and right wing decreases the wing effective angle of attack thus increasing the negative lift of the horizontal stabilisers.

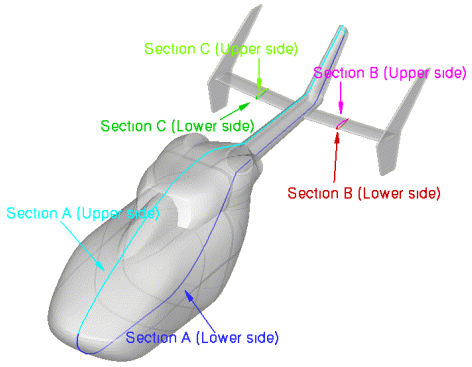

Figure 15: Surface sections on which the pressure coefficient 2D plots have been drawn.

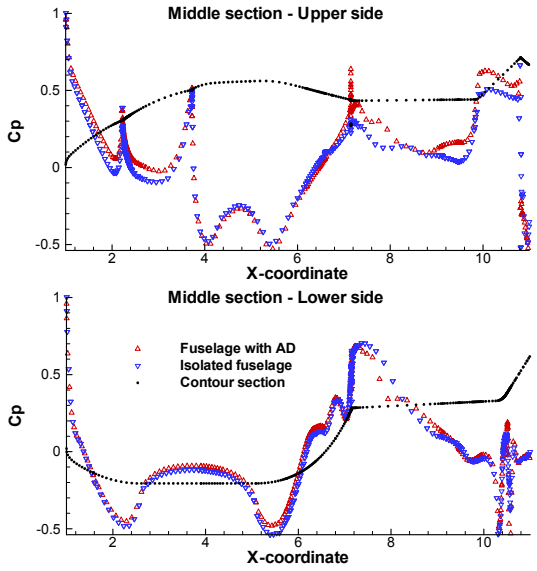

Figure 16: Pressure coefficient distribution on the fuselage middle section (Section A-upper and -lower).

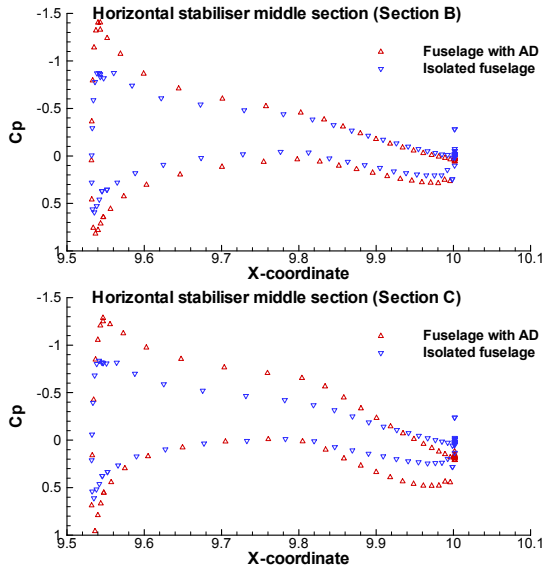

Figure 17: Pressure coefficient distribution on the middle section of the left (Section B) and right (Section C) horizontal stabiliser.

Figure 18 shows the TPL (Total Pressure Losses) on the fuselage middle plane for both cases with AD, *top picture*, and without, *bottom one*. The positive values of the TPL indicate a decrease of the total pressure, whereas negative ones indicate an increase. It becomes evident here, that the actuator disk placed right above the helicopter fuselage accelerates the flow through the disk causing an increase of the total pressure above the free stream value. The AD induced flow velocity modifies the flow quantities particularly on the engine cowling fairing and the horizontal and vertical stabilisers.

Figure 19 shows the TPL distribution on transversal planes through the helicopter fuselage and further downstream for fuselage plus AD, *top picture*, and for the isolated fuselage, *bottom one*. The vortical field generated by the AD is evident here. The asymmetry of the disk loading (see Figure 12) produces a non-symmetrical vortical field. The top-picture shows a more pronounced re-circulation on the blade retreating side (helicopter left side). Moreover the vortical patterns generated by the fuselage back door and empennage are considerably modified in both strength and shape.

In conclusion, by integrating the AD boundary condition to an isolated fuselage computation it is possible to take into account the main rotor induced velocity field on the fuselage components during a CFD computation. The main rotor/fuselage interaction phenomenon is qualitatively captured. However, although desirable, a quantitative accurate verification would be very expensive. In fact the validation of this boundary condition will require wind tunnel measurements on a full helicopter configuration, *i.e.* at least main rotor and fuselage, in which global loads, pressure distribution on both fuselage and lifting surfaces, and PIV measurements in the field, shall be recorded at a frequency of at least 72ω, so that a time average operation on the measured quantities is meaningful.

A more accurate validation of the AD model integrated in FLOWer has been presented in [7] around the Dauphin 365N configuration described in [10] for which more exhaustive wind tunnel measurements are available, such as pressure measurements on the fuselage and PIV in the field.

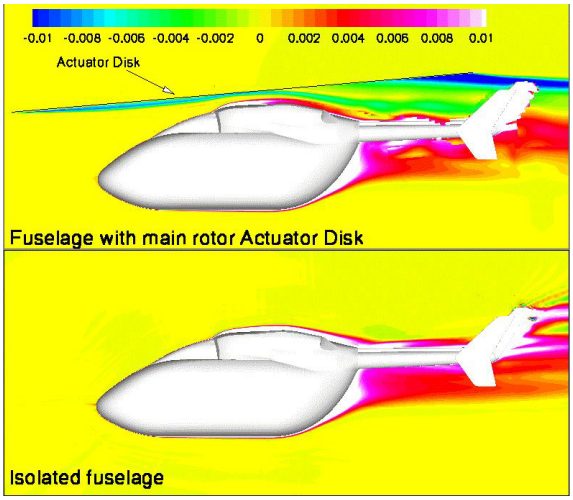

Figure 18: Total Pressure Losses distribution on the middle longitudinal fuselage section, with (upper) and without (lower) AD.

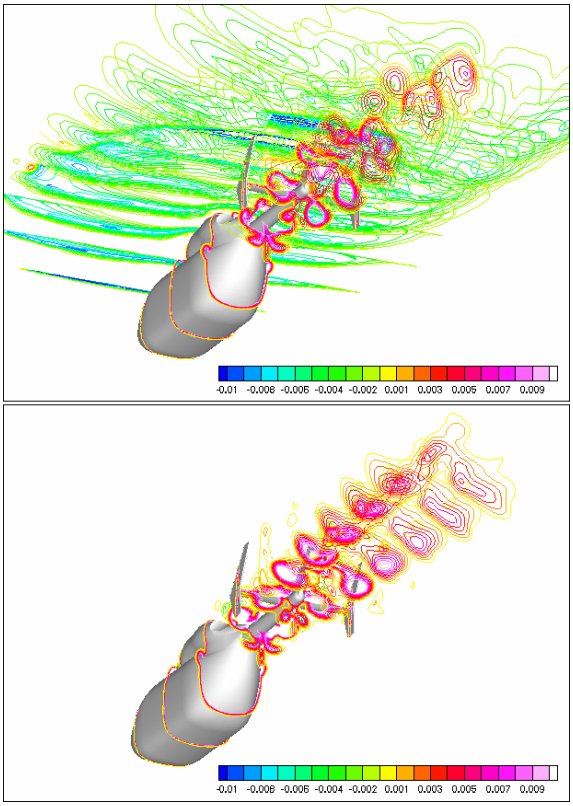

Figure 19: Total Pressure Losses distribution behind the fuselage, with (upper) and without (lower) AD.

5 Conclusions

The paper has presented the CFD analysis about the EC145 helicopter isolated fuselage and fuselage plus main rotor modelled by an actuator disk. The first part of the paper has presented the validation of the FLOWer code against wind tunnel measurements. The comparison between lift and drag coefficients is satisfactory, especially for negative angle of attack, *i.e.* the fuselage operational range, where the computed values match the wind tunnel measurements. The actuator disk model shows qualitatively meaningful results around the EC145 fuselage. A reliable quantitative validation of this test case would be very onerous.

In conclusion, thanks to the large progress in CFD tools (numerical model, convergence techniques, parallel computation, etc) and in computer performance, it is nowadays possible to predict numerous complex aerodynamic phenomena with enough accuracy and within an acceptable feedback calculation time, *i.e.* less than 3 days in industrial environment. CFD tools will help investigating some very complex phenomena usually difficult or expensive to analyse with wind tunnel facilities alone. They seem to be mature enough to drive optimisation design and thus to dramatically reduce development costs.

References

[1] A. D´Alascio, K. Pahlke, C. Castellin and M. Costes "Aerodynamics of Helicopters. Application of the Navier-Stokes Codes developed in the Framework of the Joined German/French CFD Research Program CHANCE", Proceedings of the 27th European Rotorcraft Forum, Moscow, Russia, September 2001.

[2] E. Schöll, "Numerical simulation of the BK117 / EC145 Fusealge Flow Field.", Proceedings of the 25th European Rotorcraft Forum, Rome, Italy, September 1999.

[3] G. Arnaud, A. D'Alascio, C. Castellin, L. Sudre, J.-M. Rodriguez, "*The Helicostation – A necessary computing environment for CFD applications in industry",* Proceedings of the 27th European Rotorcraft Forum, Moscow, Russia, September 2001.

[4] A. D'Alascio and A. Berthe, "Industrial use of Computational Fluid Dynamics in the helicopter design process", Presented at the International 58th Annual Forum of the American Helicopter Society, Montréal, Quebec, Canada, June 11–13, 2002.

[5] N. Kroll, C.-C. Rossow, K. Becker and F. Thiele *"The MEGAFLOW Project" Aerospace Sciences Technology Vol. 4 (2000),* pages 223-237.

[6] N. Kroll, B. Eisfeld, and H.M. Bleecke. "*The Navier-Stokes Code FLOWer", volume 71 of Notes on Numerical Fluid Mechanics,* pages 58-71. Vieweg, Braunschweig, 1999.

[7] F. Le Chuiton, "*Actuator Disc Modelling for Helicopter Rotors*", Proceedings of the 28th European Rotorcraft Forum, Bristol, UK, September 2002.

[8] A. D'Alascio, C. Castellin, M. Costes and K. Pahlke, "*Aerodynamics of Helicopter. Application of the Navier-Stokes Codes developed in the Framework of the joined German/French CFD Research Program CHANCE",* Presented at the CEAS Aerospace Aerodynamics Research Conference, Cambridge, UK, June 2002.

[9] W. Johnson, "*CAMRAD II. Comprehensive Analytical Model of Rotorcraft Aerodynamics and Dynamics",* Johnson Aeronautics, Palo Alto, California. Distributed by Analytical Methods Inc. Redmonds Washington, US.

[10] J. Brézillon, "*Simulation of RotorßFuselage Interaction by using n Actuator Disk*", Proceedings of the 26th European Rotorcraft Forum, The Hague, The Netherlands, September 2000.